Journal of Materials Chemistry A

Accepted Manuscript

ROYAL SOCIETY OF CHEMISTRY

www.rsc.org/materialsA

Journal Name

RSCPublishing

ARTICLE

Co-sensitization of 3D Bulky Phenothiazine-cored Photosensitizer with Planar Squaraine Dye for Efficient Dye-Sensitized Solar Cells

Cite this: DOI: 10.1039/x0xx00000x

Received 00th January 2012,
Accepted 00th January 2012

DOI: 10.1039/x0xx00000x

www.rsc.org/

Yong Hua,[a] Lawrence Tien Lin Lee,[b] Caishun Zhang,[c] Jianzhang Zhao,[c] Tao Chen,[*b] Wai-Yeung Wong,[*a] Wai-Kwok Wong,[*a] and Xunjin Zhu[*a]

A series of new phenothiazine-cored 3D bulky organic sensitizers **TP1–TP4** have been prepared and employed in dye-sensitized solar cells (DSSCs). The 3D bulky configuration of these molecules can effectively retard the charge recombination at the TiO_2/electrolyte interface. Amongst the four dyes, the co-adsorbent-free DSSC based on dye **TP3** exhibited the best conversion efficiency (η) of 8.00%. Subsequently, the photosensitizer **TP3** with strong UV-visible absorption and excellent performance in adsorbent-free DSSC was co-sensitized with a near-infrared (NIR) absorbing squaraine dye **YR6** to realize a UV-visible-NIR light-harvesting, which can effectively suppress the dye aggregation of **YR6** with a planar structure and retard the charge recombination in DSSC as prepared. Upon optimization, the co-sensitized DSSCs exhibited remarkable overall efficiency enhancements of 33% and 356% as compared with the devices based on **TP3** and **YR6** alone, respectively, and a high efficiency up to 9.84% was achieved at the **TP3**/**YR6** molar ratio of 25:1.

Introduction

Dye-sensitized solar cells (DSSCs) have been recognized as one of the promising alternatives to the traditional costly inorganic silicon-based solar cells due to their cost-efficient fabrication and unlimited variety of dyes available.[1] Several recent major advances in the design of dyes and electrolytes for DSSCs have led to record power conversion efficiencies.[2] However, the rapid progress of perovskite solar cells raised some doubts on whether the efficiency of the conventional DSSCs could be improved highly enough through current research strategies. In view of the theoretical performance and the best achieved values in different kinds of solar cells, there is still a big room for the improvement of DSSC performance by increasing the short circuit current (J_{SC}), open circuit voltage (V_{OC}) and fill fact (FF). The major strategy to increase the J_{SC} is to improve the light harvesting efficiency by developing organic dyes with UV-visible-near-infrared (NIR) light-harvesting capability.[3] Unfortunately, designing a single small molecule dye that can efficiently absorb panchromatic sunlight is still challenging. Co-sensitization of the TiO_2 electrode by two or more dyes with complementary spectral profile has been demonstrated to be an effective strategy to realize a UV-visible-NIR spectral response and increase the photocurrent of organic dyes-based DSSC. To date, most of those successful co-sensitized DSSCs reported have combined a ruthenium dye or a porphyrin dye with metal-free organic dyes.[2,4] In our previous works, a series of simple phenothiazine-based dyes have ever been developed for highly efficient DSSC applications.[5] And the co-sensitization of the simple organic dye with a NIR-absorbing porphyrin dye can greatly retard the back reaction and enhance the spectral response of solar cells, resulting in an efficiency (η) exceeding 10%.[6] Notably, squaraine (SQ) based dyes have been wildly applied as NIR photosensitizers because of their extraordinary intense absorption in the NIR spectral region and photolytic stability.[7] Nazeeruddin et al. used a squaraine dye (**SQ1**) in combination with a metal-free dye (**JK2**) to obtain higher efficiency (η = 7.38%) than the individual dye-based cells.[7d] Han et al. employed a *cis*-configured squaraine dye (**HSQ1**) together with **N3** for the co-sensitized solar cell; the action spectra (IPCE) was extended up to 800 nm, and the efficiency over 8.14% was achieved.[8] Nevertheless, SQs-based co-sensitized device performances were usually not as good as expected. The major factors for the relatively poor performances were the weak absorption of SQs below 500 nm, the formation of aggregates on TiO_2 surface that induce quenching of photo-excited states and quick charge recombination,[9] indicating that there is still much room to further improve the device performance by structural engineering of the organic dyes to broaden the light absorption, and suppress the dye aggregation of SQs and retard the charge recombination.

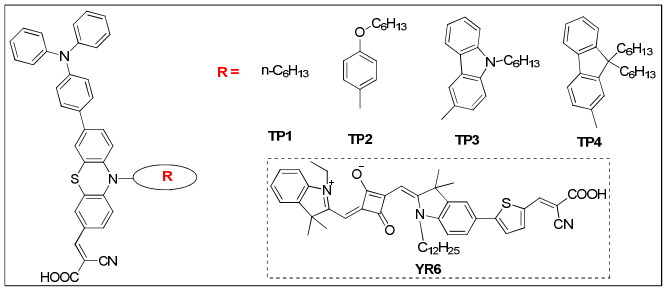

Figure 1. Structures of **TP1**–**TP4** and **YR6.**

In this contribution, a series of phenothiazine-cored 3D bulky organic dyes have been designed and prepared, in which the dyes consist of the cyanoacrylate acceptor directly attached to the C(3) position of phenothiazine, and the triphenylamine (TPA) donor group at C(7) on the opposite side of the acceptor, and the bulky substituent Ar of different size, i.e., hexyl, hexyloxybenzene, hexylcarbazole, and dihexylfluorene at N(10) of the phenothiazine periphery (**Figure 1**). The influence of 3D bulky substituent on the suppression of dye aggregation and charge recombination as well as photovoltaic performance of DSSCs was systematically investigated. Amongst them, the dye **TP3** with the highest efficiency of 8%, was used to co-sensitize with an NIR-absorbing squaraine dye, **YR6**.[10] The co-sensitized devices based on **TP3** and **YR6** dyes show significantly enhanced J_{sc} relative to the individual single-dye sensitized devices. Upon optimization, the device made at the **TP3/YR6** molar ratio in a 25:1 ratio yielded J_{sc} = 19.18 mA cm^{-2}, V_{oc} = 0.721 V, FF = 0.712 and η = 9.84%; The performance is far superior to that of the single-dye device made from either **TP3** (η = 8.00%) or **YR6** (η = 2.16%) under the same conditions. The efficiency of 9.84% is the highest reported efficiency for squaraine dyes-based co-sensitized DSSCs. And electrochemical impedance analysis and transient photovoltage studies were performed to elucidate the high performance of the co-sensitized DSSCs.

2. Results and Discussion

2.1. Synthesis and Characterization

The NIR dye **YR6** was prepared according to the literature (see Supporting Information).[10] The synthetic protocols towards these new dyes **TP1–TP4** are depicted in Scheme S1. The dyes **TP1–TP4** were prepared in good yields through the Suzuki cross coupling of (4-(diphenylamino)phenyl)boronic acid with 7-bromo-*N*-hexyl-10*H*-phenothiazine-3-carbaldehyde and its analogues, respectively, followed by the widely employed Knoevenagel condensation with cyanoacetic acid in the presence of ammonium acetate. All the new intermediates and target dye molecules were fully characterized by ^{1}H NMR, ^{13}C NMR and mass spectral data.

2.2. UV-Vis Absorption Properties

The absorption spectra of **TP1–TP4** in CH_2Cl_2 are displayed in **Figure 2a** and the detailed spectroscopic data are collected in **Table 1**. These dyes display two prominent distinct absorption bands in the range of 400~600 nm. The shorter wavelength bands are ascribed to the localized aromatic π-π* electronic transitions of the chromophores, while the longer wavelength ones correspond to the intramolecular charge transfer (ICT) from the donor to the acceptor. The ICT peaks (λ_{max}) for **TP2** (485 nm), **TP3** (491 nm) and **TP4** (487 nm) show a red-shift compared to that of **TP1** (469 nm), indicating that the incorporation of stronger electron-donating groups onto the nitrogen atom of phenothiazine core is beneficial to light-harvesting capability. In addition, the corresponding molar extinction coefficients of **TP1–TP4** for the visible absorption peaks are 2.17, 1.99, 2.28 and 1.89 × 10^4 M^{-1} cm^{-1}, respectively. And TP3 appended with hexylcarbazole unit possesses the best light-harvesting property, which may be beneficial for photocurrent generation in DSSCs. The absorption bands of **TP1-TP4** adsorbed onto nanocrystalline TiO_2 surface display slight blue-shifts with respect to those in solutions, which can be ascribed to the deprotonation of carboxylic acid, as well as to the formation of H-aggregation on the semiconductor surface for most organic dyes of this type (**Figure 2**b).[11] Notably, the maximum absorption peaks of **TP2**, **TP3** and **TP4** exhibit much less hypsochromic shift relative to that of **TP1**, which demonstrate that the intermolecular π-stacked aggregations on TiO_2 films may be effectively weakened in the presence of these bulky auxiliary substituents on the nitrogen atom of phenothiazine core.

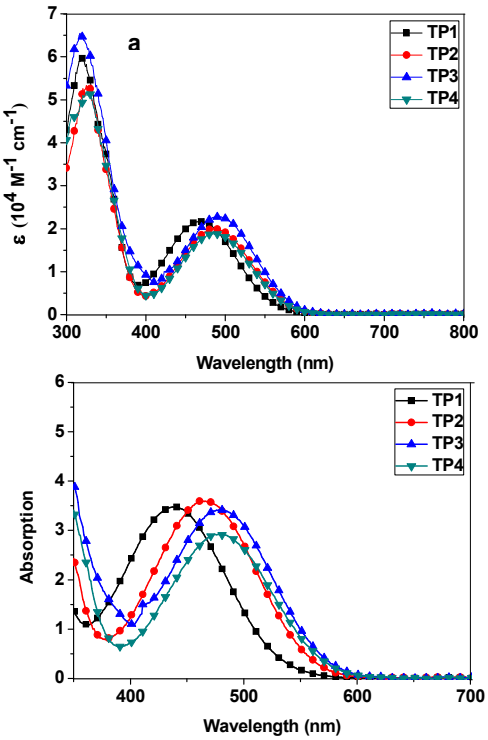

Figure 2. Absorption spectra of **TP1–TP4** in CH_2Cl_2 solutions (a) and on TiO_2 films (b).

2.3. Electrochemical Properties

To study the possibility of electron injection from the excited state of photosensitizers into the conduction band (CB) of TiO_2 semiconductor and dye regeneration by redox electrolytes, the electrochemical behaviors of **TP1–TP4** were studied by cyclic voltammetry in CH_2Cl_2 solutions (**Figure 3**). Obviously, all of the four dyes exhibit three quasi-reversible oxidation waves. Their first redox waves are attributed to the oxidations of the arylamino moiety. The second and the third quasi-reversible redox waves correspond to the phenothiazine segment. The first oxidation potentials (E_{ox}) correspond to HOMOs, while the LUMOs are calculated from the values of E_{ox} and the zero-zero band gaps ($E_{0\text{-}0}$) estimated from the onset of the UV-visible absorption spectra. The electrochemical data of the four dyes

are listed in **Table 1**. The estimated HOMO levels of the four dyes are sufficiently lower than the electrolyte iodide/tri-iodide redox potential value (0.4 V vs. NHE), thus ensuring the oxidized dyes could be efficiently regenerated by the electrolyte. On the other hand, the LUMO levels of all dyes lie above the conduction band edge (CB) of TiO_2 (−0.5 V vs. NHE), indicating that the electron injection from the excited dye molecules into the conduction band of TiO_2 is energetically permitted.

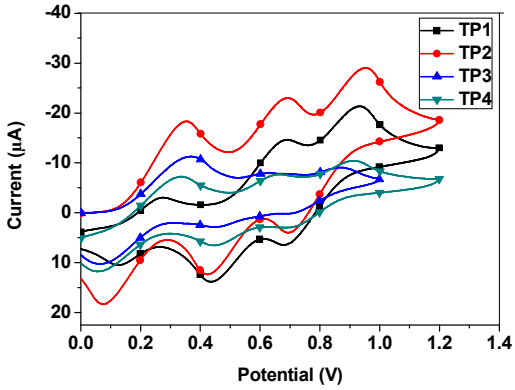

Figure 3. Cyclic voltammograms of **TP1–TP4** in CH_2Cl_2 solution.

Table 1. Absorption and electrochemical parameters for **TP1–TP4**.

Compd.	λ_{max} [a] ($\varepsilon/10^4$ $M^{-1}cm^{-1}$) /nm	λ_{max} [b] /nm	E_{ox} [c] / V	$E_{0\text{-}0}$ [d] / eV	E_{red} [e] / V
TP1	469 (2.17)	436	0.70	2.21	–1.51
TP2	478 (1.99)	465	0.78	2.18	–1.40
TP3	491 (2.28)	481	0.80	2.14	–1.34
TP4	487 (1.89)	480	0.76	2.15	–1.39

[a] Absorption maximum in 1×10^{-5} mol L^{-1} CH_2Cl_2 solution. [b] Absorption maximum on TiO_2 film. [c] Oxidation potential in CH_2Cl_2 solution containing 0.1 M $(n\text{-}C_4H_9)_4NPF_6$ were calibrated with ferrocene (0.4 V vs. NHE) and taken as the HOMO. [d] $E_{0\text{-}0}$ was determined from the onset of absorption spectrum. [e] $E_{red} = E_{ox} - E_{0\text{-}0}$.

2.4. Theoretical Calculation

To better understand the electronic distribution in the frontier molecular orbitals and electronic processes upon photoexcitation, the density functional theory (DFT) calculations were performed using Gaussian 03 program package at the B3LYP/6-31 G(d)* hybrid functional for full geometrical optimization (**Figure 4**). The HOMOs are delocalized along the donor group and phenothiazine core, while the LUMOs are primarily located over the cyanoacrylic acid segment and partly on the phenothiazine core. Hence, the well-overlapped HOMO and LUMO orbitals on the phenothiazine core can guarantee a fast charge transfer transition between donor and acceptor. Thus, excitation from the HOMO to the LUMO should lead to efficient photoinduced electron transfer from the electron-donating triphenylamine moiety to the terminal cyanoacrylic acid, and finally into the conduction band of TiO_2.

In the optimized ground-state geometries shown in **Figure S1**, the dihedral angles formed between the different size of bulky substituents (hexyloxybenzene, hexylcarbazole, and dihexylfluorene) at N(10) of the phenothiazine periphery and the phenothiazine core are computed to be 90° for **TP2–TP4**. Obviously, the whole molecular skeletons of the four dyes show out-of-plane twist conformation. Notably, **TP3** and **TP4** show considerably large bulky "space", of which the 3D twisted structure is favorable for suppressing dye aggregation, charge recombination, and back-electron transfer.[12]

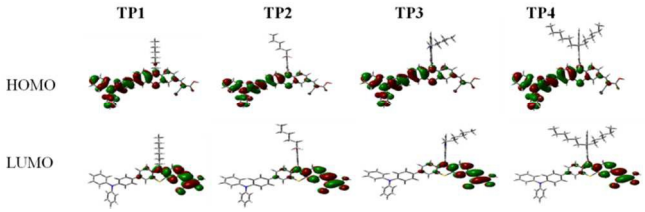

Figure 4. Calculated frontier orbitals for dyes **TP1–TP4.**

2.5. Photovoltaic Performance

The action spectra of incident photon-current conversion efficiencies (IPCEs) for DSSCs based on **TP1–TP4** are plotted in **Figure 5**a. The IPCEs of the four dyes display broad bands in the region of 300–650 nm with values mostly > 60 to 70%. It is worth noting that the onset of their IPCE curves of **TP2-TP4** show obvious red-shifts to longer wavelength compared with that of **TP1**. This further demonstrates that the 3D constructed organic dyes tend to form a broad IPCE, which is consistent with their visible absorption spectrum.

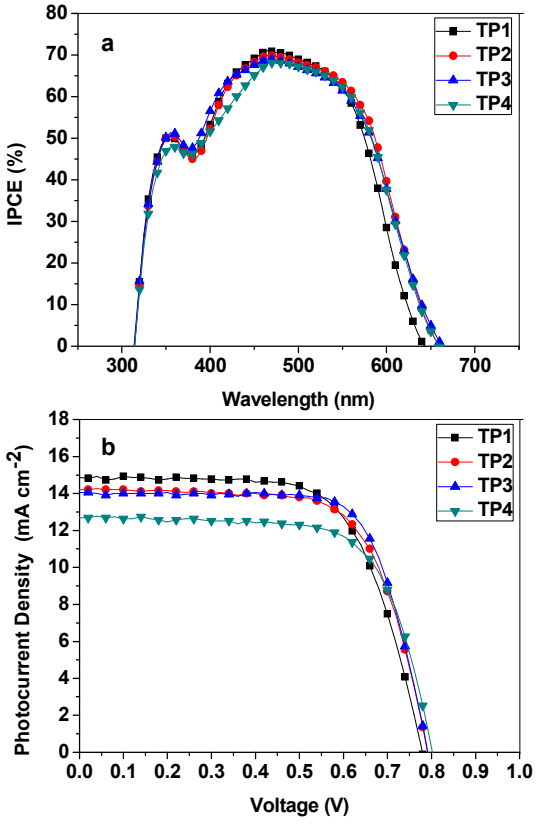

Figure 5. IPCE spectra (a) and $J-V$ curves (b) for DSSCs sensitized by **TP1–TP4**.

Among these dyes, the DSSC based on **TP3** exhibited the best photovoltaic performance with J_{sc} = 14.06 mA cm^{-2}, V_{oc} = 0.791 V, FF = 0.719, corresponding to the power conversion efficiency (η) of 8.00% (**Figure 5b** and **Table 2**). Under the same conditions, other cells sensitized with the dyes **TP1**, **TP2** and **TP4** also showed attractive performances with J_{sc} of 14.87,

14.21 and 12.68 mA cm^{-2}, V_{oc} of 0.778, 0.790 and 0.801 V, and *FF* of 0.666, 0.686 and 0.693, corresponding to the η values of 7.71%, 7.70% and 7.05%, respectively. The most inferior photocurrent for **TP4**-based solar cell is most likely attributed to its lowest dye loading (**Table 2**). The four photosensitizers exhibited relatively high V_{oc} values in I^-/I_3^- based DSCs, in the range of 0.778–0.801 V. As compared to **TP1**, 3D structural **TP2**, **TP3** and **TP4** show higher V_{oc} values. This can be attributed to the suppression of charge recombination at the TiO_2/dye/electrolyte interface by incorporating 3D bulky conjugated substituents on the *N*-atom of phenothiazine core. The results illustrate that the introduction of the bulky substituents in π-conjugated spacer on the orthogonal direction could suppress dye aggregation and retard charge recombination in DSSCs more effectively than the linear alkyl chain.

Table 2. Photovoltaic parameters of DSSCs under full sunlight illumination (AM 1.5G, 100 mW cm^{-2})[a]

Dye	Dye loading capacity/mol cm^{-2}	J_{sc}/mA cm^{-2}	V_{oc}/V	FF	η/%
TP1	3.98×10^{-7}	14.87	0.778	0.666	7.71
TP2	3.56×10^{-7}	14.21	0.790	0.686	7.70
TP3	3.03×10^{-7}	14.06	0.791	0.719	8.00
TP4	2.87×10^{-7}	12.68	0.801	0.693	7.05

[a] Performance of DSSCs measured in a 0.24 cm^2 working area on a FTO substrate at room temperature. Dyes were maintained at 0.5 mM in acetonitrile/*tert*-butyl alcohol (volume ratio, 1:1) for **TP1**–**TP4** dyes. Electrolyte: LiI (0.05 M), I_2 (0.1 M), and DMPII (0.6 M) in acetonitrile/*tert*-butyl alcohol (1:1, v/v).

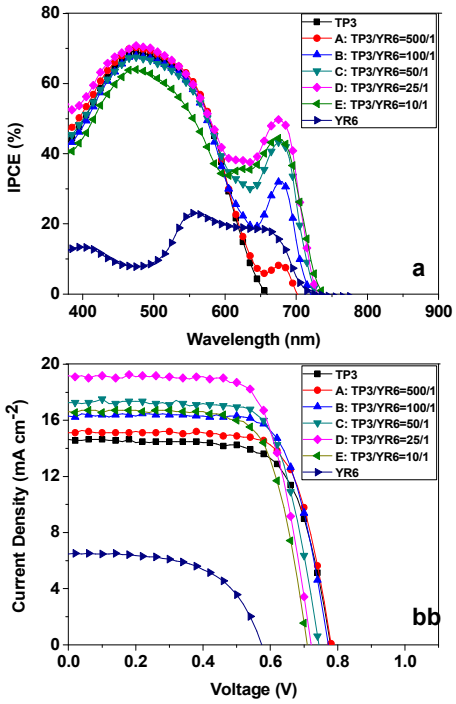

Figure 6. IPCE spectra (a) and J–V curves (b) of DSSCs based on **TP3**, **YR6** and co-sensitization of the two dyes.

2.6. Photophysical and Photovoltaic Performance of DSSCs based on Co-sensitization of TP3 and YR6

In order to realize a panchromatic absorption in DSSCs, the reported NIR dye **YR6** was selected to co-sensitize with **TP3** to enhance the light harvesting efficiency due to their complementary absorption properties**. Figure S2** shows the co-adsorption spectrum of the two dyes on TiO_2 films immersed in **TP3** and **YR6** solutions at varied molar ratios. The spectrum shows a broad absorption from 400 nm to 750 nm. And the absorption of co-sensitized films displayed an obvious enhancement of light absorption in the NIR region when compared with the individually sensitized films. Notably, the absorption peaks in the NIR region was red-shifted by 10 nm after co-sensitization, which indicates that the adsorption of **TP3** could largely suppress the aggregation of NIR dye YR6 on the TiO_2 surface as a consequence of the 3D bulky repulsion by **TP3**. At the same time, the light harvesting efficiency can be effectively improved by the co-sensitization of **TP3** and **YR6** with complementary absorption bands.

The IPCE spectra of devices sensitized by **TP3**, **YR6** and co-sensitization of the two dyes are plotted as a function of excitation wavelength and presented in **Figure 6a**. The IPCE spectra of **TP3/YR6** co-sensitized DSSCs show an impressive panchromatic response from 300 to 750 nm. As expected, the IPCE performances of co-sensitized DSSCs are better than that of the cells based on **TP3** and **YR6** alone. Also, it was found that the IPCE of the co-sensitized devices were strongly dependent on the molar ratio of the two dyes in solutions. When the co-sensitized cell was prepared at the **TP3/YR6** molar ratio of 25:1, the device gave the largest IPCE increase in the 650-750 nm region from ~20% to ~50%, which contributes to the higher photocurrent.

The *J*–*V* curves for the cells based on **TP3**, **YR6** and co-sensitization of the two dyes are presented in **Figure 6**b and the photovoltaic data are summarized in **Table 3**. The η of the devices based on individual **TP3** and **YR6** are 8.00 % and 2.16 %, respectively. To optimize the co-sensitization process for better photovoltaic performance, we investigated five devices at different dye-loading molar ratios, coded as A–E. It was observed that all of the co-sensitized solar cells showed much higher photocurrent and efficiency than those of the individual dye-sensitized solar cells. The performance of device A containing **TP3** and **YR6** in a solution of molar ratio 500:1 led to the η value of 8.58%, and it was increased to 9.17% for device B and 9.28% for device C when the devices were prepared at the TP3/YR6 molar ratio 100:1 and 50:1, respectively. When the TP3/YR6 molar ratio reached 25:1, the device D yielded the best performance with a short circuit current density of 19.18 mA cm^{-2}, an open circuit voltage of 0.721 V and a fill factor of 0.712, corresponding to an overall conversion efficiency of 9.84%. A further increase of the **TP3/YR6** molar ratio to 10:1 (device E) led to a decreased efficiency of 8.42%. The observed trend is qualitatively consistent with the photoresponse capabilities of the five devices as illustrated by IPCE spectra.

Electrochemical Impedance Spectroscopies (EIS) analysis has been performed to elucidate the interfacial charge recombination process under a forward bias of −0.73 V in the dark. As shown in **Figure 7**a, a major semicircle for each device was observed in the Nyquist plot, which is related to the resistance of charge transfer processes at the dye/TiO_2/electrolyte interface, *i.e.,* the recombination kinetics between the charge on TiO_2 film and I_3^- species from the electrolyte.[13] In general, the resistance value (R_{rec}) corresponds to the diameters of the semicircles; a smaller R_{rec} value indicates a faster charge recombination, thus giving a lower V_{oc}.[14] The R_{rec} values for these devices increase in the order E < D < C < B < A. The trend observed here is consistent with the results yielded for the V_{oc} values, *i.e.*, the V_{oc} values increased

from 0.709 V to 0.780 V with increasing molar concentration of **TP3** from 10:1 to 500:1. The results suggest that the usage of **TP3** with 3D structure can form a good blocking layer between TiO_2 and the electrolyte, suppressing the charge recombination between the injected electron in TiO_2 conduction band and I_3^- in the electrolyte. Though the co-adsorbent of YR6 sacrificed the photovoltage, the photocurrent related to the light-harvesting capability was strengthened significantly, resulting in a highly improved photovoltaic efficiency.

Table 3. Photovoltaic performances of DSSCs based on **TP3**, **YR6** and co-sensitization of the two dyes.[a]

Device	Dye-loading strategy	J_{sc} /mAcm^{-2}	V_{oc} /V	*FF*	η /%
TP3	0.5 mM	14.06	0.791	0.719	8.00
YR6	0.5 mM	6.47	0.572	0.584	2.16
A	TP3/YR6(500:1)	15.12	0.780	0.728	8.58
B	TP3/YR6(100:1)	16.31	0.771	0.729	9.17
C	TP3/YR6(50:1)	17.27	0.743	0.723	9.28
D	TP3/YR6(25:1)	19.18	0.721	0.712	9.84
E	TP3/YR6(10:1)	16.63	0.709	0.699	8.42

[a] Performance of DSSCs measured in a 0.24 cm^2 working area on a FTO (8 Ω/square) substrate at room temperature. **TP3** (0.5 mM) and **YR6** (0.5 mM) were maintained in acetonitrile:*tert*-butyl alcohol solution (volume ratio, 1:1). Electrolyte: LiI (0.05 M), I_2 (0.1 M), and DMPII (0.6 M) in acetonitrile/*tert*-butyl alcohol (1:1, v/v).

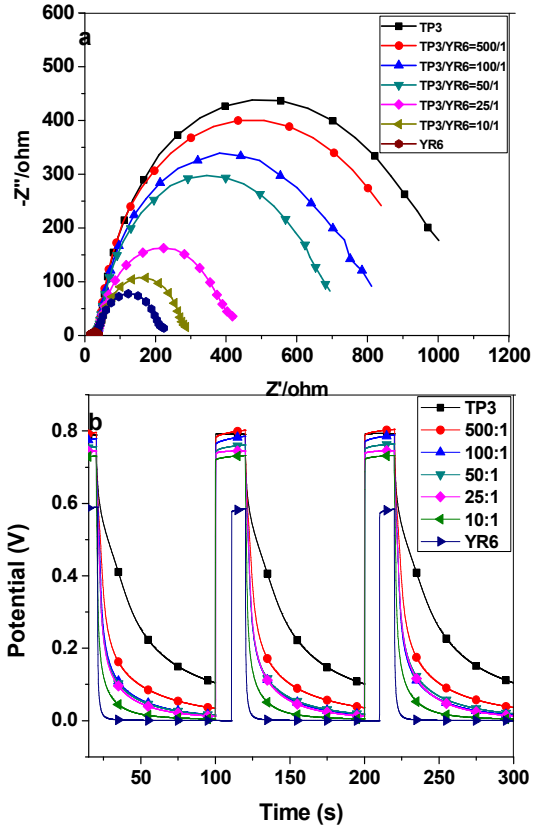

Figure 7. EIS Nyquist plots (a) and open circuit voltage decay profiles (b) for DSSCs based on these devices.

To further probe the charge recombination kinetics of the devices, open circuit voltage decay (OCVD) was recorded to illustrate the lifetime of V_{oc} from an illuminated quasi-equilibrium state to dark equilibrium. **Figure 7**b shows the OCVD profiles of devices A to E. The correlation between V_{oc} decay and electron lifetime (τ_n) can be described by the following equation:

$$\tau_n = -\frac{K_B T}{e}\left(\frac{dV_{oc}}{dt}\right)^{-1}$$

where K_B is the Boltzmann constant, T is temperature, and e is the positive elementary charge.[15] Therefore, the electron lifetimes in solar cells can be extracted from the slope of V_{oc} decay curves. As a consequence, when the devices were prepared at different **TP3/YR6** molar ratio from 500:1 to 10:1, the slope became steeper and steeper, indicating that the electron lifetimes were gradually reduced with the decrease in the molar concentration of **TP3**. These are well consistent with the EIS spectra that decreasing molar concentration of **TP3** would lead to the faster charge recombination at the interface.

3. Conclusions

In conclusion, we have successfully developed a series of new 3D bulky phenothiazine-cored organic photosensitizers for DSSC applications. Compared with **TP1**, **TP2–TP4** featuring a 3-dimensional bulky structure exhibited a bathochromic shift in wavelength on TiO_2 films, and the suppression of dye aggregation and reduced charge recombination, leading to better DSSC performance. Impressively, the co-adsorbent-free DSSCs based on **TP3** showed the highest efficiency of 8.00%. Subsequently, the organic dye **TP3** with strong UV-visible absorption and excellent performance in co-adsorbent-free DSSC was co-sensitized with the near-infrared (NIR) absorbing squaraine dye **YR6** to realize a UV-visible-NIR light-harvesting capability, which effectively suppressed the dye aggregation of **YR6** with a planar structure and retarded the charge recombination in co-sensitized DSSCs. Upon optimization, the co-sensitized DSSCs exhibited remarkable overall efficiency enhancements of 33% and 356% as compared with the devices based on the **TP3** and **YR6** alone, respectively, and the highest PCE of 9.84% was achieved at the **TP3/YR6** molar ratio of 25:1. To our knowledge, such a value of η also represents the highest reported efficiency ever reported in the literature for the squaraine dye-based co-sensitized DSSCs.

4. Experimental Section

Materials and Reagents. All solvents and reagents were purchased from Sigma-Aldrich Company and used as received without further purification. The starting material phenothiazine and 2-cyanoacetic acid were purchased commercially. TiO_2 paste and iodide-based liquid electrolyte (HL-HPE) were purchased from Dyesol company. The synthetic routes of phenothiazine-based dyes **TP1–TP4** are outlined in **Scheme S1** and the details are depicted.

General procedures for the preparation of TP1–TP4
A mixture of each of the precursors 4a–4d (0.20 mmol) and cyanoacetic acid (89 mg, 1.10 mmol) in acetic acid (20 mL) was refluxed in the presence of ammonium acetate (200 mg) overnight under a N_2 atmosphere. Then, water was added and extracted with CH_2Cl_2. Next, the solvent was removed under vacuum and the crude compound was purified by column

chromatography on silica gel eluting with CH_2Cl_2/MeOH (20:1, v/v) to give TP1-TP4 as a dark red solid.

(*E*)-2-Cyano-3-(7-(4-(diphenylamino)phenyl)-10-hexyl-10H-phenothiazin-3-yl)acrylic acid (TP1)
Yield: 80 mg (62%). ^{1}H NMR (400 MHz, DMSO-d_6, δ): 8.15 (s, 1H), 7.90-7.93 (m, 1H), 7.81 (d, J = 2.0 Hz, 1H), 7.54 (d, J = 2.0 Hz, 2H), 7.44-7.47 (m, 1H), 7.40 (d, J = 2.0 Hz, 1H), 7.31 (t, J = 7.6 Hz, 4H), 7.12 (d, J = 7.6 Hz, 1H), 6.98-7.09 (m, 10H), 3.93 (t, J = 6.8 Hz, 4H), 1.66-1.71 (m, 2H), 1.36-1.41 (m, 2H), 1.24-1.26 (m, 4H), 0.83 (t, J = 6.8 Hz, 3H). ^{13}C NMR (400 MHz, DMSO-d_6, δ): 163.77, 152.34, 148.44, 146.98, 146.55, 141.32, 134.95, 132.41, 131.59, 129.54, 129.03, 127.01, 125.49, 124.49, 124.08, 123.99, 123.23, 123.18, 122.65, 122.51, 116.84, 116.60, 115.46, 99.61, 46.95, 30.77, 26.00, 25.68, 22.06, 13.81. HRMS (MALDI-TOF, *m/z*): [M^+] calcd for $C_{40}H_{35}N_3O_2S$, 621.2444; found, 621.2440.

(*E*)-2-Cyano-3-(7-(4-(diphenylamino)phenyl)-10-(4-(hexyloxy)phenyl)-10H-phenothiazin-3-yl)acrylic acid (TP2)
Yield: 76 mg (59%). ^{1}H NMR (400 MHz, DMSO-d_6, δ): 8.00 (s, 1H), 7.70 (s, 1H), 7.51 (d, J = 8.8 Hz, 1H), 7.44-7.46 (m, 2H), 7.27-7.32 (m, 7H), 7.13-7.18 (m, 3H), 6.98-7.04 (m, 6H), 6.93 (d, J = 8.8 Hz, 2H), 6.08 (d, J = 8.8 Hz, 2H), 4.01 (t, J = 6.0 Hz, 2H), 1.70-1.73 (m, 2H), 1.21-1.41 (m, 6H), 0.85 (t, J = 4.0 Hz, 3H). ^{13}C NMR (400 MHz, DMSO-d_6, δ): 163.70, 158.77, 151.74, 147.13, 146.92, 146.55, 140.80, 135.00, 134.86, 132.24, 131.46, 131.31, 131.15, 129.52, 128.00, 126.90, 125.55, 125.06, 124.03, 123.85, 123.22, 123.15, 118.63, 118.41, 116.82, 116.63, 115.09, 99.89, 67.82, 31.01, 28.63, 25.23, 22.09, 13.93. HRMS (MALDI-TOF, *m/z*): [M^+] calcd for $C_{46}H_{39}N_3O_3S$, 713.2707; found, 713.2739.

(*E*)-2-Cyano-3-(7-(4-(diphenylamino)phenyl)-10-(9-hexyl-9H-carbazol-3-yl)-10H-phenothiazin-3-yl)acrylic acid (TP3)
Yield: 89 mg (71%). ^{1}H NMR (400 MHz, DMSO-d_6, δ): 8.03 (s, 1H), 7.69 (t, J = 8.8 Hz, 2H), 7.50 (d, J = 8.8 Hz, 2H), 7.27-7.34 (m, 7H), 6.99-7.09 (m, 12H), 6.94 (d, J = 8.0 Hz, 2H), 6.11-6.18 (m, 2H), 4.46 (t, J = 6.0 Hz, 2H), 1.80-1.88 (m, 2H), 1.35-1.42 (m, 2H), 1.21-1.28 (m, 4H), 0.82 (t, J = 6.8 Hz, 3H). ^{13}C NMR (400 MHz, DMSO-d_6, δ): 163.76, 162.27, 151.97, 147.66, 147.15, 146.99, 146.94, 146.56, 145.89, 141.24, 140.71, 139.98, 139.53, 134.98, 132.28, 131.10, 129.52, 127.54, 127.11, 126.88, 125.01, 124.29, 124.03, 123.93, 123.75, 123.43, 123.25, 123.15, 122.89, 122.47, 119.22, 118.60, 118.32, 116.77, 115.52, 100.10, 30.94, 30.67, 28.57, 26.16, 22.03, 13.82. HRMS (MALDI-TOF, *m/z*): [M^+] calcd for $C_{52}H_{42}N_4O_2S$, 786.3023; found, 786.2978.

(*E*)-2-Cyano-3-(10-(9,9-dihexyl-9H-fluoren-2-yl)-7-(4-(diphenylamino)phenyl)-10H-phenothiazin-3-yl)acrylic acid (TP4)
Yield: 82 mg, (68%). ^{1}H NMR (400 MHz, DMSO-d_6, δ): 8.08 (d, J = 8.0 Hz, 1H), 8.00 (s, 1H), 7.87-7.89 (m, 1H), 7.70 (d, J = 2.0 Hz, 1H), 7.52-7.54 (m, 2H), 7.43-7.45 (m, 3H), 7.32-7.36 (m, 4H), 7.24-7.28 (m, 4H), 6.92-7.08 (m, 9H), 6.07-6.11 (m, 2H), 1.97 (t, J = 6.0 Hz, 4H), 0.94-1.02 (m, 12H), 0.64 (t, J = 6.8 Hz, 6H), 0.52 (t, J = 6.8 Hz, 4H). ^{13}C NMR (400 MHz, DMSO-d_6, δ): 163.64, 153.59, 152.44, 151.49, 150.56, 146.90, 146.82, 146.59, 141.46, 140.67, 139.50, 137.73, 135.07, 132.11, 130.68, 129.52, 128.86, 128.56, 127.92, 127.13, 126.82, 125.68, 124.90, 124.20, 124.06, 123.93, 123.18, 122.87, 122.45, 120.37, 118.50, 118.38, 116.82, 116.38, 114.78, 101.84, 55.14, 30.83, 30.68, 28.78, 23.37, 21.79, 13.74. HRMS (MALDI-TOF, *m/z*): [M^+] calcd for $C_{59}H_{55}N_3O_2S$, 869.4009; found, 869.4047.

Characterizations. ^{1}H and ^{13}C NMR spectra were recorded with a Bruker Ultrashield 400 Plus NMR spectrometer. The high-resolution matrix-assisted laser desorption/ ionization time of flight (MALDI-TOF) mass spectra were obtained with a Bruker Autoflex MALDI-TOF mass spectrometer. The UV-visible absorption spectra of these dyes were measured in CH_2Cl_2 solution with a Varian Cary 100 UV-Vis spectrophotometer. The cyclic voltammograms (CV) were measured with Versastat II electrochemical work station using a normal three-electrode cell with a Pt working electrode, a Pt wire auxiliary electrode and a saturated Ag/Ag^+ reference electrode in KNO_3 aqueous solution, 0.1 M tetra-*n*-butylammonium hexafluorophosphate ($TBAPF_4$) was used a supporting electrolyte in CH_2Cl_2 solution. The potential of the reference electrode was calibrated by ferrocene after each set of measurements, and all potentials mentioned in the work were against normal hydrogen electrode.

Fabrication and characterization of cells. To make a reasonable comparison, all the anode films for the DSSC were made under the same standard manner, which are composed of 12 μm thick of transparent layer (TiO_2 with diameter of 20 nm) and 6 μm thick of scattering layer (TiO_2 nanoparticles with diameter of 200 nm). In specific, a doctor-blade technique was utilized to prepare photoanode (TiO_2) films. Firstly, a layer of ca. 6 μm TiO_2 paste (20 nm) was doctor-bladed onto the FTO conducting glass and then relaxed at room temperature for 3 min before heating at 150 °C for 6 min. This procedure was repeated once to achieve a film thickness of ca. 12 μm and the resulting surface was finally coated by a scattering layer (ca. 6 μm) of TiO_2 paste (200 nm). The electrodes were gradually heated under an air flow at 275 °C for 5 min, 325 °C for 5 min, 375 °C for 5 min and 470 °C for 30 min to remove polymers and generate three-dimensional TiO_2 nanoparticle network. After that, the sintered films were soaked with 0.02 M TiF_4 aqueous solution for 45 min at 70°C, washed with deionized water, and further annealed at 450 °C for 30 min. After cooling down to ca. 80°C, the electrodes were immersed into a 5×10^{-4} M **TPn** or 5×10^{-4} M **YR6** dye bath in acetonitrile/*tert*-butyl alcohol (volume ratio, 1:1) solution and maintained in the dark for 16 h. For the co-sensitized solar cells, **TP3** and **YR6** dyes of the same concentration (5×10^{-4} M) were mixed in different volume ratios, 500:1, 100:1, 50:1, 25:1 and 10:1. Afterwards, the electrodes were rinsed with ethanol to remove the non-adsorbed dyes and dried in air. Pt counter electrodes were prepared by sputtering method at 15 mA for 90 s at a power of 150 W. Two holes (0.75 mm in diameter) were pre-drilled in the FTO glass for introducing the electrolyte. The dye-adsorbed TiO_2 electrode and Pt-counter electrode were assembled into a sandwich type cell and sealed with a hot-melt parafilm at about 100 °C. The liquid electrolyte consisting of 0.6 M 1,2-dimethyl-3-propylimidazolium iodide (DMPII), 0.1 M LiI, 0.05 M I_2 in a mixture of acetonitrile and *tert*-butyl alcohol (volume ratio, 1:1) was introduced into the cell through the drilled holes at the back of the counter electrode. At last, the holes were sealed by parafilm and covering glass (0.1 mm thickness) at an elevated temperature. The effective areas of all the TiO_2 electrodes were 0.24 cm^2. The current−voltage (J−V) characteristics of the assembled DSSCs were measured by a semiconductor characterization system (Keithley 236) at room temperature in air under the spectral output from solar simulator (Newport)

using an AM 1.5G filter with a light power of 100 mW cm^{-2}. IPCEs of DSSCs were recorded in Solar Cell QE/IPCE Measurement System (Zolix Solar Cell Scan 100) using DC mode. CHI 660D electrochemical workstation was used to characterize the electrochemical properties of the DSSCs. Electrochemical impedance spectroscopy (EIS) was recorded under dark condition over a frequency range of 0.1-10^5 Hz with an AC amplitude of 10 mV and the parameters were calculated from Z-View software (v2.1b, Scribner AssociatNe, Inc.).

Acknowledgments

We thank Hong Kong Research Grants Council (HKBU202210, HKBU202811 and HKBU203011) and Hong Kong Baptist University (FRG2/14-15/034 and FRG1/14-15/058) for the financial support. W.-K.W. and W.-Y.W. also thank a grant from Areas of Excellence Scheme, University Grants Committee, Hong Kong (Project No. [AoE/P-03/08]). W.-Y.W. thanks The Science, Technology and Innovation Committee of Shenzhen Municipality (JCYJ20120829154440583) for financial support and Dalian University of Technology (Haitian Scholarship for W.-Y.W.). X. D. X and T. C acknowledge the financial support from the CUHK Group Research Scheme and CUHK Focused Scheme B Grant ''Center for Solar Energy Research''.

Notes and references

[a] *Institute of Molecular Functional Materials, Department of Chemistry and Institute of Advanced Materials, Hong Kong Baptist University, Waterloo Road, Kowloon Tong, Hong Kong, P. R. China. Fax: 852 3411 7048; Tel: 852 34115157; E-mail: xjzhu@hkbu.edu.hk; wkwong@hkbu.edu.hk; rwywong@hkbu.edu.hk.*

[b] *Department of Physics, the Chinese University of Hong Kong, Shatin, New Territories, Hong Kong, P. R. China. Fax: 852 2603 5204; Tel: 852 3943 6278; E-mail: taochen@phy.cuhk.edu.hk*

[c] *State Key Laboratory of Fine Chemicals, School of Chemical Engineering, Dalian University of Technology, Dalian, 116024, P. R. China.*

1 a) B. O'Regan and M. Grätzel, *Nature*. 1991, **353**, 737; b) M. Grätzel, *Nature*, 2001, **414**, 338; c) A. Hagfeldt and M. Grätzel, *Acc. Chem. Res*. 2000, **33**, 269; d) M. Grätzel, *Acc. Chem. Res*. 2009, **42**, 1788; e) A. Hagfeldt, G.Boschloo, L. C. Sun, L. Kloo and H. Pettersson, *Chem. Rev*. 2010, **110**, 6595.

2 A. Yella, H. W. Lee, H. N. Tsao, C. Y. Yi, A. K. Chandiran, M. K. Nazeeruddin, E. W. G. Diau, C. Y. Yeh, S. M. Zakeeruddin and M. Grätzel, *Science*, 2011, **334**, 629.

3 a) H. Tian, X. Yang, R. Chen, A. Hagfeldt and L. Sun, *Energy Environ. Sci*. 2009, **2**, 674. b) S. Kim, G. K. Mor, M. Paulose, O. K. Varghese, C. Baik and C. A. Grimes, *Langmuir*. 2010, **26**, 13486; c) J. H. Yum, P. Walter, S. Huber, D. Rentsch, T. Geiger, F. Nuesch, F. D. Angelis, M. Grätzel and M. K. Nazeeruddin, *J. Am. Chem. Soc*. 2007, **129**, 10320. d) P. K. Sudeep, K. Takechi and P. V. Kamat, *J. Phys. Chem. C*. 2007, **111**, 488. e) S. Kolemen, O. A. Bozdemir, Y. Cakmak, G. Barin, S. Erten-Ela, M. Marszalek, J. H. Yum, S. M. Zakeeruddin, M. K. Nazeeruddin, M. Grätzel and E. U. Akkaya, *Chem. Sci*. 2011, **2**, 949. f) Y. Hua, H. D. Wang, X. J. Zhu, A. Islam, L. Y. Han, C. J. Q, W. Y. Wong and W. K. Wong, *Dyes Pigments*, 2014, **102**, 196. g) C. J. Qin, A. Mirloup, N. Leclerc, A. Islam, A. El-Shafei, L. Y. Han and R. Ziessel, *Adv. Energy Mater*, 2014, DOI: 10.1002/aenm.201400085.

4 a) L. Y. Han, A. Islam, H. Chen, C. Malapaka, B. Chiranjeevi, S. F. Zhang, X. D. Yang and M. Yanagida. *Energy Environ. Sci*. 2012, **5**, 6057. b) C. M. Lan, H. P. Wu, T. Y. Pan, C. W. Chang, W. S. Chao, C. T. Chen, C. L. Wang, C. Y. Lin and E. W. G. Diau, *Energy Environ. Sci.* 2012, **5**, 6460.

5 Y. Hua, S. Chang, D. D. Huang, X. Zhou, X. J. Zhu, J. Z. Zhao, T. Chen, W. Y. Wong and W. K. Wong, *Chem. Mater*. 2013, **25**, 2146.

6 S. Chang, H. D. Wang, Y. Hua, Q. Li, X. D. Xiao, W. K. Wong, W. Y. Wong, X. J. Zhu and T. Chen, *J. Mater. Chem. A*. 2013, **1**, 11553.

7 a) M. Gsänger, E. Kirchner, M. Stolte, C. Burschka, V. Stepanenko, J. Pflaum and F. Würthner, *J. Am. Chem. Soc*, 2014, **136**, 2351. b) J. Y. Li, C. Y. Chen, C. P. Lee, S. C. Chen, T. H. Lin, H. H. Tsai, K. C. Ho and C. G. Wu, *Org. Lett*, 2010, **12**, 5454. c) U. Mayerhöffer, K. Deing, K. Gru, H. Braunschweig, K. Meerholz and F. Würthner, *Angew. Chem. Int. Ed*. 2009, **48**, 8776. d) H. Choi, S. Kim, S. O. Kang, J. Ko, M. S. Kang, J. N. Clifford, A. Forneli, E. Palomares, M. K. Nazeeruddin and M. Grätzel, *Angew. Chem. Int. Ed*. 2008, **47**, 8259.

8 C. J. Qin, Y. Numata, S. F. Zhang, X. D. Yang, A. Islam, K. Zhang, H. Chen and L. Y. Han, *Adv. Funct. Mater*. 2013, **24**, 3059.

9 a) K. Funabiki, H. Mase, Y. Saito, A. Otsuka, A. Hibino, N. Tanaka, H. Miura, Y. Himori, T. Yoshida, Y. Kubota and M. Matsui, *Org. Lett*. 2012, **14**, 1246. b) S. Paek, H. Choi, C. Kim, N. Cho, S. So, K. Song, M. K. Nazeeruddinc and J. Ko, *Chem. Commun*. 2011, **47**, 2874. c) C. J. Qin, W. Y. Wong and L. Y. Han, *Chem. Asian J*. 2013, **8**, 1706.

10 Y. R. Shi, R. B. M. Hill, J. H. Yum, A. Dualeh, S. Barlow, M. Grätzel, S. R. Marder and M. K. Nazeeruddin, *Angew. Chem. Int. Ed*. 2011, **50**, 6619.

11 a) Y. Z. Wu, X. Zhang, W. Q. Li, Z. S. Wang, H. Tian and W. H. Zhu, *Adv. Energy Mater*. 2012, **2**, 149. b) L. P. Cai, H. N. Tsao, W. Zhang, L. Wang, Z. S. Xue, M. Grätzel and B. Liu, *Adv. Energy Mater*. 2013, **3**, 200.

12 a) G. Li, M. Liang, H. Wang, Z. Sun, L. N. Wang, Z. H. Wang and S. Xue, *Chem. Mater*. 2013, **25**, 1713. b) J. Tang, J. L. Hua, W. J. Wu, J. Li, Z. G. Jin, Y. T. Long and H. Tian, *Energy Environ. Sci*. 2010, **3**, 1736. c) M. F. Xu, D. F. Zhou, N. Cai, J. Y. Liu, R. Z. Li and P. Wang, *Energy Environ. Sci*. 2011, **4**, 4735.

13 a) H. H. Chou, Y. C. Chen, H. J. Huang, T. H. Lee, J. T. Lin, C. Tsaic and K. Chen, *J. Mater. Chem*. 2012, **22**, 10929. b) Q. Wang, J. E. Moser and M. Grätzel, *J. Phys. Chem. B*. 2005, **109**, 14945. c) Y. Hua, S. Chang, H. D. Wang, D. D. Huang, J. Z. Zhao, T. Chen, W. Y. Wong, W. K. Wong and X. J. Zhu, *J. Power. Sources*. 2013, **243**, 253. d) K. Pei, Y. Z. Wu, W. J. Wu, Q. Zhang, B. Q. Chen, H. Tian and W. H. Zhu, *Chem. Eur. J*. 2012, **18**, 8190.

14 a) Y. Hua, S. Chang, J. He, C. S. Zhang,; J. Z. Zhao, T. Chen, W. Y. Wong, W. K. Wong and X. J. Zhu, *Chem. Eur. J*. 2014, **20**, 6300. b) Q. Wang, J. Moser and M. Grätzel, *J. Phys. Chem. B*. 2005, **109**, 14945. c) J. B. Yang, F. L. Guo, J. L. Hua, X. Li, W. J. Wu, Y. Qu and H. Tian, *J. Mater. Chem*. 2012, **22**, 24356.

15 a) A. Zaban, M. Greenshtein and J. Bisquert, *ChemPhysChem*. 2003, **4**, 859. b) J. Bisquert, A. Zaban, M. Greenshtein and I. Mora-Seró, *J. Am. Chem. Soc*. 2004, **126**, 13550.